Proceedings of the
International Conference on Mechanical Engineering 2005
(ICME2005) 28- 30 December 2005, Dhaka, Bangladesh

ICME05-FL-19

NUMERICAL STUDY OF HETEROGENEOUS CONDENSATION IN THE TRANSONIC FLOW FIELDS

Shigeru Matsuo[1], Masanori Tanaka[2], Miah MD. Ashraful Alam[2], MD. Mahbubul Alam[2] and Toshiaki Setoguchi[1]

[1] Deptartment of Mechanical Engineering, Saga University, 1 Honjo-machi, Saga-shi, Saga 840-8502, Japan.
[2] Graduate School of Science and Technology, Saga University, 1 Honjo-machi, Saga-shi, Saga 840-8502, Japan.

ABSTRACT

In the present study, the effect of the heterogeneous condensation on the characteristics of unsteady shock wave generated on the bump model in the transonic flow field was investigated numerically. As a result, it was found that the condensation with heterogeneous nucleation had a strong effect on the whole flow field, and it reduced the strength of the shock. Furthermore, the total pressure loss was dependent on the concentration of the solid particles per unit volume.

Keywords: Compressible Flow, Transonic Flow, Heterogeneous Condensation, Simulation.

1. INTRODUCTION

The transonic flow over an airfoil is characterized by a shock wave standing on the suction surface. Here, the interaction between the shock wave and boundary layer becomes complex because the shock wave imposes an adverse pressure gradient on the boundary layer. It was found in the previous works [1, 2] that the occurrence of homogeneous condensation just before the shock wave not only led to the reduction of the shock strength but also suppressed the oscillation of shock wave.

Condensation phenomenon in a high speed flow field is induced through the homogeneous condensation process [3]. In this process, condensation nuclei are generated by collision and aggregation of vapor molecules. The condensation of the vapor, so called homogeneous condensation, takes place on the nuclei. In heterogeneous condensation, however, the condensation of the vapor takes place on foreign nuclei [4] : smoke and vapor from fires and various industries, dust from land surfaces, salt from oceans and particulate products from chemical reaction. Their presence in sufficient numbers leads to the condensation near to equilibrium at a degree of supersaturation slightly larger than unity.

In the present study, a condensing flow was produced by an expansion of moist air with solid particles in the nozzle with circular bump model, and an unsteady shock wave occurred in the supersonic parts of the flow fields. The numerical investigation is carried out to clarify the effect of the heterogeneous condensation on the characteristics of the unsteady shock wave.

2. NUMERICAL METHOD

Assumptions in the present calculation are as follows : both velocity slip and temperature difference do not exist among condensate droplets, solid particles and inert gas mixture, and the effects of the condensate droplets and solid particles on pressure are neglected. All particles are assumed to have a smooth and spherical shape, and all condensation nuclei are assumed to be chemically inert and insoluble in water vapor.

The governing equations are unsteady two-dimensional compressible Navier-Stokes equations and a rate of liquid-phase production with homogeneous and heterogeneous nucleations [5, 6]. They are written in the two-dimensional Cartesian coordinate system (x,y) as follows :

$$\frac{\partial \boldsymbol{U}}{\partial t}+\frac{\partial \boldsymbol{E}}{\partial x}+\frac{\partial \boldsymbol{F}}{\partial y}=\frac{1}{Re}\left(\frac{\partial \boldsymbol{R}}{\partial x}+\frac{\partial \boldsymbol{S}}{\partial y}\right)+\boldsymbol{Q} \qquad (1)$$

where $\boldsymbol{U}$ is the vector of conservative variables, $\boldsymbol{E}$ and $\boldsymbol{F}$ are inviscid flux vectors, and $\boldsymbol{R}$ and $\boldsymbol{S}$ are viscous flux vectors. $\boldsymbol{Q}$ is the source term corresponding to additional equations. Each vector is given by

$$\boldsymbol{U}=\begin{bmatrix}\rho_m\\ \rho_m u\\ \rho_m v\\ E_t\\ \rho_m g_{hom}\\ \rho_m n_{hom}\\ \rho_m g_{het}\\ \rho_m k_{het}\end{bmatrix},\ \boldsymbol{E}=\begin{bmatrix}\rho_m u\\ \rho_m u^2+p\\ \rho_m uv\\ u(E_t+p)\\ \rho_m u g_{hom}\\ \rho_m u n_{hom}\\ \rho_m u g_{het}\\ \rho_m u k_{het}\end{bmatrix},\ \boldsymbol{F}=\begin{bmatrix}\rho_m v\\ \rho_m uv\\ \rho_m v^2+p\\ v(E_t+p)\\ \rho_m v g_{hom}\\ \rho_m v n_{hom}\\ \rho_m v g_{het}\\ \rho_m v k_{het}\end{bmatrix},$$

$$\boldsymbol{R}=\begin{bmatrix}0\\ \tau_{xx}\\ \tau_{xy}\\ u\tau_{xx}+v\tau_{yx}+k\dfrac{\partial T}{\partial x}\\ 0\\ 0\\ 0\\ 0\end{bmatrix},\quad \boldsymbol{S}=\begin{bmatrix}0\\ \tau_{yx}\\ \tau_{yy}\\ u\tau_{xy}+v\tau_{yy}+k\dfrac{\partial T}{\partial y}\\ 0\\ 0\\ 0\\ 0\end{bmatrix} \tag{2}$$

$$\boldsymbol{Q}=\begin{bmatrix}0\\ 0\\ 0\\ 0\\ \dfrac{4\pi}{3}\rho_l\left(r^{*}_{hom}{}^{3}\cdot I_{hom}+3\rho_m\cdot n_{hom}\cdot r_{hom}{}^{2}\cdot\dfrac{dr_{hom}}{dt}\right)\\ I_{hom}\\ (1-z)\cdot\dfrac{\pi}{3}\cdot(1-\cos\theta)^2\cdot(2+\cos\theta)\cdot\rho_l\cdot\\ \left(r^{*}_{het}{}^{3}\cdot\tilde{I}_{het}\cdot A_e\cdot n_{het}+3\rho_m\cdot k_{het}\cdot r_{het,emb}{}^{2}\cdot\dfrac{dr_{het,emb}}{dt}\right)\\ +z\cdot 4\pi\cdot\rho_l\cdot n_{het}\cdot r_{het,nuc}{}^{2}\cdot\dfrac{dr_{het,nuc}}{dt}\\ I_{het}\end{bmatrix} \tag{3}$$

where g_{hom} and g_{het} are condensate mass fractions generated by homogeneous and heterogeneous condensations, respectively. I_{het} and $\tilde{I}_{het}$ denote the rates of formation of critical clusters per unit volume of moist air and unit surface area of the solid particle, respectively [4, 6]. Therefore, the total flow rate of liquid phase g_{total} is written as [6]

$$g_{total}=g_{hom}+g_{het} \tag{4}$$

Both of the condensate mass fractions g are expressed as a rate equation, based on the following equation [5].

$$\frac{dg}{dt}=\frac{4\pi}{3}\cdot\rho_l\cdot r^{*}(t)^3\cdot\frac{I(t)}{\rho_m(t)}+\int_{-\infty}^{t}4\pi\cdot\rho_l\cdot\frac{I(\tau_t)}{\rho_m(\tau_t)}\cdot\frac{\partial r(t,\tau_t)}{\partial t}\cdot r(t,\tau_t)^2\cdot d\tau_t \tag{5}$$

In Eqs.(2) and (3), n_{hom} is the number of condensate droplet generated by homogeneous nucleation per unit mass of moist air, and k_{het} is the number of embryos generated on the surface of solid particle by heterogeneous nucleation per unit mass of moist air. E_t and p in Eq.(2) are total energy per unit volume and pressure, respectively. τ_{xx}, τ_{xy}, τ_{yx} and τ_{yy} are the components of viscous shear stress. Subscripts m and l refer to mixture and liquid, respectively. k is thermal conductivity. In 5th and 6th components in Eq(3), r_{hom} and r^{*}_{hom} are the radius of nucleus and the critical droplet radius, respectively. In 7th and 8th components in Eq(3), A_e and n_{het} are the surface area of solid particle on which the vapor can nucleate and the concentration of solid particles in inert gas mixture, respectively. $r_{het,emb}$ is the radius of cap-shaped (hemispherical) embryo generated on the surface of the solid particle. θ is the contact angle between the solid particle and cap-shaped embryo. $r_{het,nuc}$ and r^{*}_{het} are the radius of nucleus covered by the liquid film and the critical droplet radius, respectively.

Heterogeneous nucleation process consists of four nucleation stages [6] as follows : I. Generation of embryo ; II. Growth of embryo ; III. Formation of liquid film ; and IV. Growth of liquid film. In the first stage, embryos are generated on the surface of a solid particle. In the second stage, embryos on the surface of a solid particle grow up and new embryos are generated on the particle. In the third stage, a liquid film is formed on the whole surface of a solid particle and the solid particle covered by the liquid film can be assumed a nucleus. In the fourth stage, the liquid film grows up.

There are two models for heterogeneous nucleation process [6]. For model 1, four nucleation stages from I to IV are considered for nucleation process. For model 2, only the fourth stage (IV) of nucleation process is used. This model is assumed that nucleation stages from I to III proceed in an infinitesimal time. In the present study, model 2 is employed as a heterogeneous condensation model because the difference between results obtained by both models is very small. In simulations, z is set at 1.0 and the 8th component in Eqs.(2) and (3) is eliminated because the nucleation for embryo does not need to be considered.

The governing equation systems for compressible viscous flow were discretized by the finite difference method. Third-order TVD finite difference scheme with MUSCL approach [7] was used for spatial derivative terms and second-order central difference scheme in discretizing viscous terms. The spatially discretized equations were integrated in time by means of a time splitting method that had the second order accuracy. Baldwin-Lomax turbulence model [8] was employed to close the governing equations.

The validity of the method used in the present simulation was confirmed by comparison with the previous study [6].

3. COMPUTATIONAL CONDITIONS

Figure 1 shows the computational grids of transonic nozzle flow field. The nozzle height H at the inlet and exit is 60.0 mm. A bump nozzle with the radius of circular arc R =100 mm was set at the lower wall in the test section. The height of nozzle throat h^{*} is 56.0 mm. The chord length (characteristic length) L is 56.0 mm. The number of grids is 250×60.

The working gas is moist air with solid particles. The

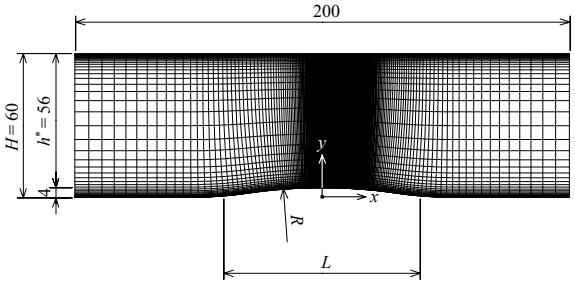

Fig 1. Computational grids (Unit : mm)

initial degree of supersaturation S_{01} of the working gas is 0.4. The concentration of the solid particles per unit volume of the moist air in the reservoir $n_{het,01}$ was changed in the range from 0 to 1.0×10^{14} m^{-3}. In the present study, the radius of the solid particles R_p and the contact angle θ were fixed at 1.0×10^{-8} m and 30 degrees, respectively [6]. Total temperature T_{01} and total pressure p_{01} in the reservoir are 298 K and 102 kPa, respectively. The inlet Mach number upstream of the bump model is 0.73.

Vectors of the conservative variables at inlet boundary were fixed at initial conditions and static pressure at the exit boundary p_{exit} was fixed constant (p_{exit}/p_{01}=0.683). Vectors of the conservative variables at a fictitious cell at inlet and exit were constrained with Riemann invariant. The non slip-wall was used as the solid wall boundary conditions. Iso-pressure and no heat transfer conditions were constrained on the solid wall. Condensate mass fraction g was set at g = 0 on the solid wall.

4. RESULTS AND DISCUSSION

Figure 2 shows the contour maps of Mach number in case of no condensation (S_{01}=0, Dry air). Flow direction is from left to right. In this case, a periodic shock oscillation with frequency $f \approx 669$ Hz occurs on the bump wall in the region close to the throat.

Figure 3 shows contour maps of Mach number in cases for homogeneous ($n_{het,01}$ = 0 m^{-3}, S_{01} = 0.4) and heterogeneous condensations ($n_{het,01}$ = 1.0×10^{11} m^{-3}, 5.0×10^{12} m^{-3} and 1.0×10^{14} m^{-3}). Flow direction is left to right. In these cases, the oscillation of the shock wave is suppressed completely due to the condensation and the configuration of the shock wave becomes small in comparison with that of dry air (Fig.2). Furthermore, it was confirmed that the shock strength was reduced with an increase in the solid particle concentration. The reason is that Mach number just before shock wave reduces due to condensation.

Figure 4 shows the contour maps of condensate mass fraction corresponding to cases shown in Fig.3. For case of homogeneous condensation (Fig.4(a)), the condensate mass fraction near the bump wall side increases from $x/L \approx 0.1$ before the shock wave and the distribution expands over downstream region. However, the distribution in

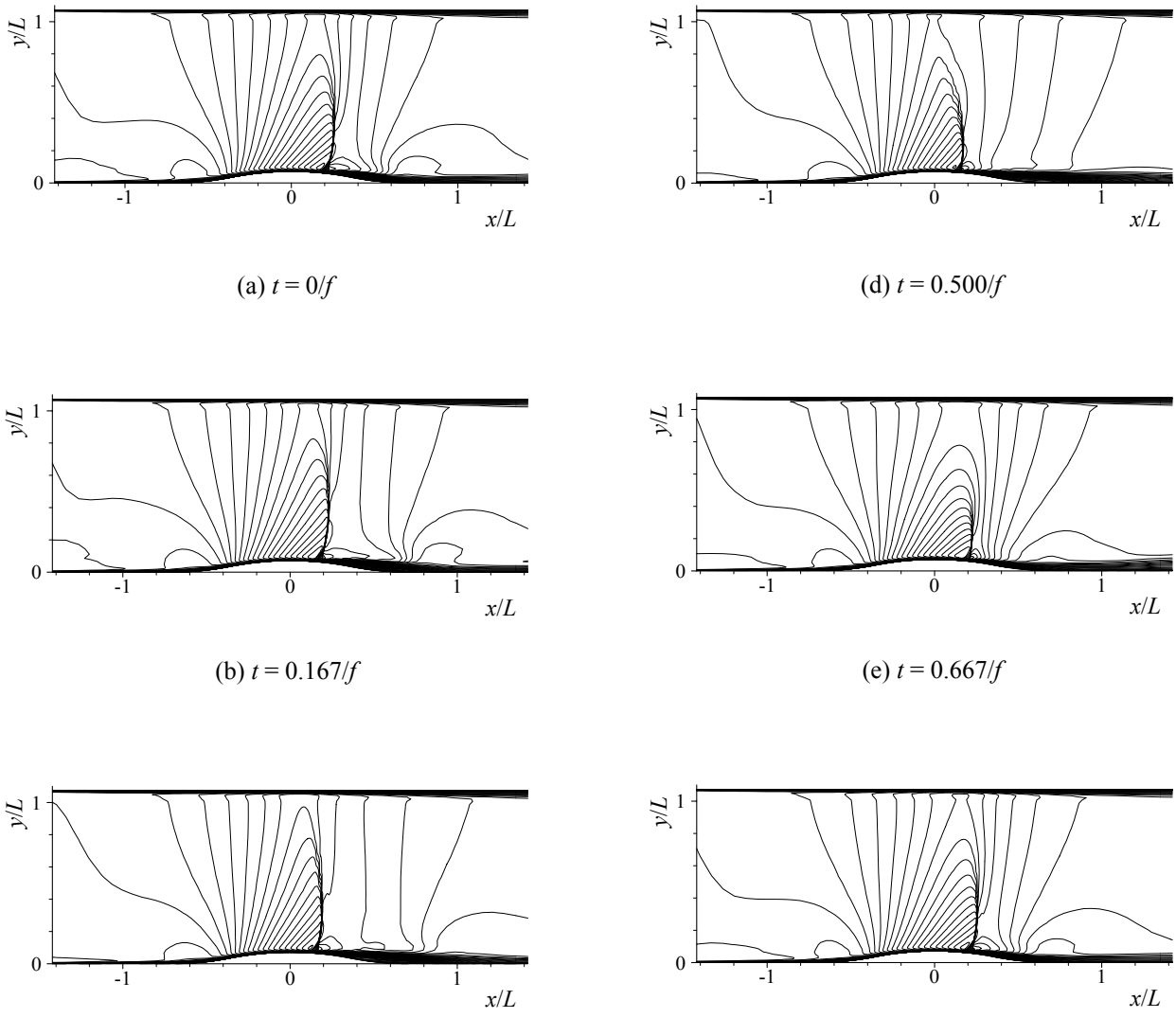

(a) $t = 0/f$ (d) $t = 0.500/f$

(b) $t = 0.167/f$ (e) $t = 0.667/f$

(c) $t = 0.333/f$ (f) $t = 0.833/f$

Fig 2. Contour maps of Mach number (Dry air)

Fig.4(b) increases from $x/L \approx -0.3$ and expands over both solid boundaries. This is due to the effect of the heterogeneous condensation. Furthermore, a rapid increase of the condensate mass fraction over the bump wall can be observed due to the occurrence of the homogeneous condensation. In Figs.4(c) and 4(d), the heterogeneous condensation occurs from upstream region in comparison with the case of Fig.4(b). Especially, the rapid increase of liquid phase due to the homogeneous condensation does not appear over the bump wall in Fig.4(d).

Figure 5 shows the distributions of nucleation rate $I_{\hom}$ for homogeneous condensation and condensate mass fraction g for $n_{het,01} = 0$ m^{-3}, 1.0×10^{11} m^{-3}, 5.0×10^{12} m^{-3} and 1.0×10^{14} m^{-3} on the measuring line shown in Fig.3(a). In each case, a large number of condensate nuclei generate above the bump wall side. In Fig.5(b), the condensate mass fraction g_{total} increases due to the heterogeneous condensation in the range of $x/L > -0.3$. Furthermore, the nucleation rate reaches a maximum at $x/L = 0.1$ and , in the range of $x/L > 0.1$, it increases steeply with the addition of homogeneous condensation. In Fig.5(c), the effect of heterogeneous condensation on the flow field become strong and the position of onset of condensation moves upstream in comparison with the case of $n_{het,01} = 1.0\times10^{11}$ m^{-3} (Fig.5(b)). For the case of

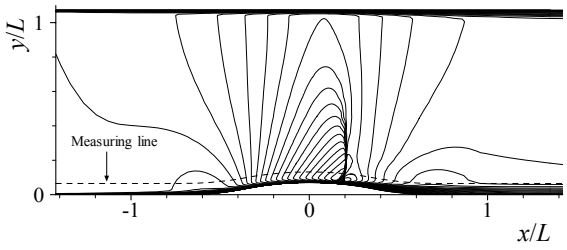

(a) Homogeneous condensation ($n_{het,01} = 0$ m^{-3})

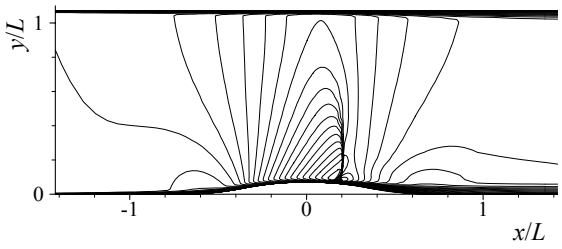

(b) $n_{het,01} = 1.0\times10^{11}$ m^{-3}

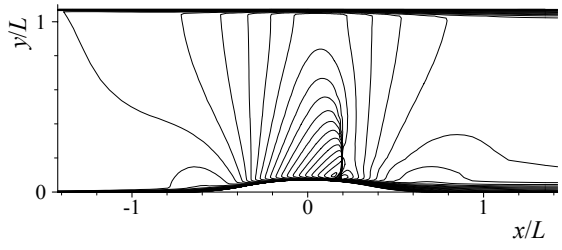

(c) $n_{het,01} = 5.0\times10^{12}$ m^{-3}

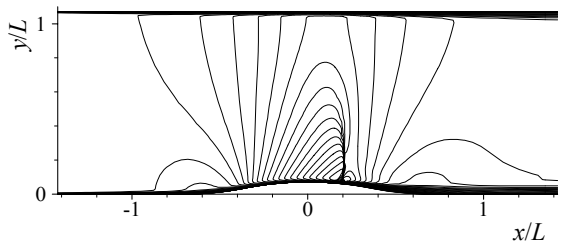

(d) $n_{het,01} = 1.0\times10^{14}$ m^{-3}

Fig 3. Contour maps of Mach number

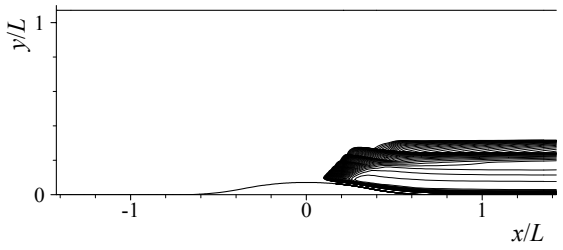

(a) Homogeneous condensation ($n_{het,01} = 0$ m^{-3})

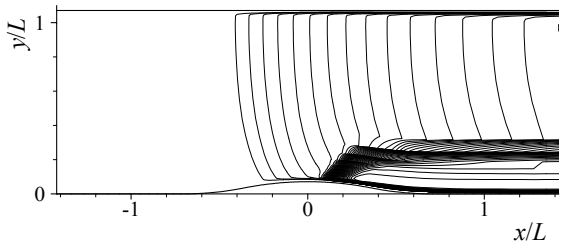

(b) $n_{het,01} = 1.0\times10^{11}$ m^{-3}

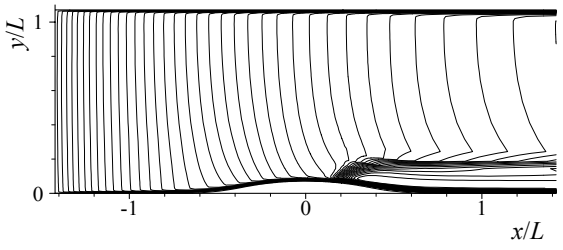

(c) $n_{het,01} = 5.0\times10^{12}$ m^{-3}

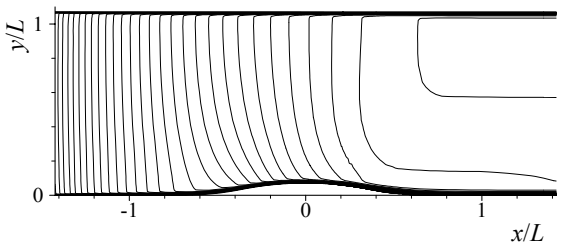

(d) $n_{het,01} = 1.0\times10^{14}$ m^{-3}

Fig 4. Contour maps of condensate mass fraction

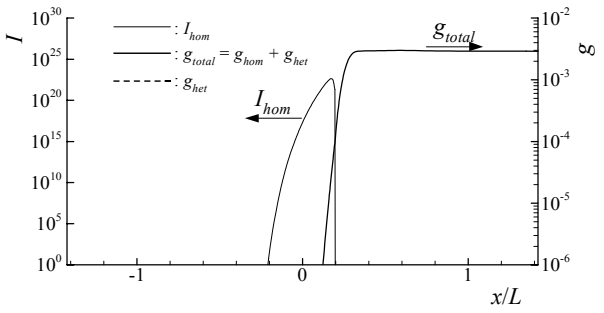

(a) Homogeneous condensation ($n_{het,01}$ = 0 m^{-3})

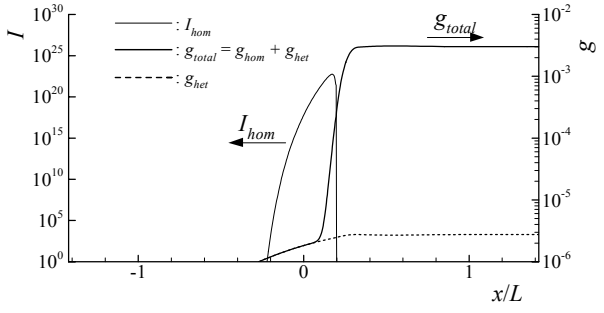

(b) $n_{het,01}$ = 1.0×10^{11} m^{-3}

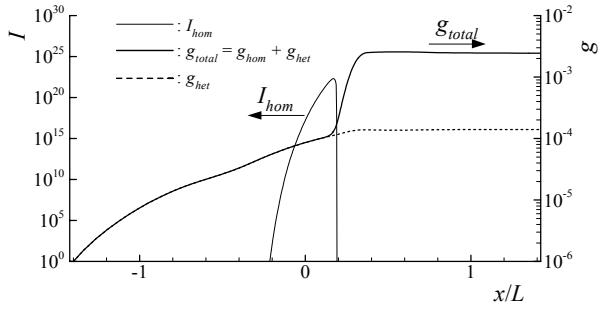

(c) $n_{het,01}$ = 5.0×10^{12} m^{-3}

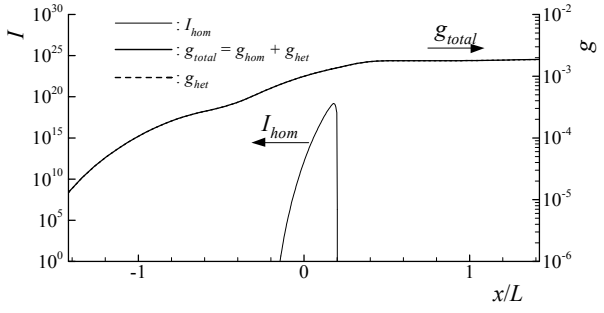

(d) $n_{het,01}$ = 1.0×10^{14} m^{-3}

Fig 5. Distributions of condensation properties

$n_{het,01}$ = 1.0×10^{14} m^{-3} (Fig.5(d)), the condensate nuclei are largely generated in the region close to the throat. However, the occurrence of the liquid phase due to the homogeneous condensation is hardly observed in the flow field, and the amount of the condensate mass fraction is larger than those of Figs.5(b) and 5(c) in the range of x/L < 0.3.

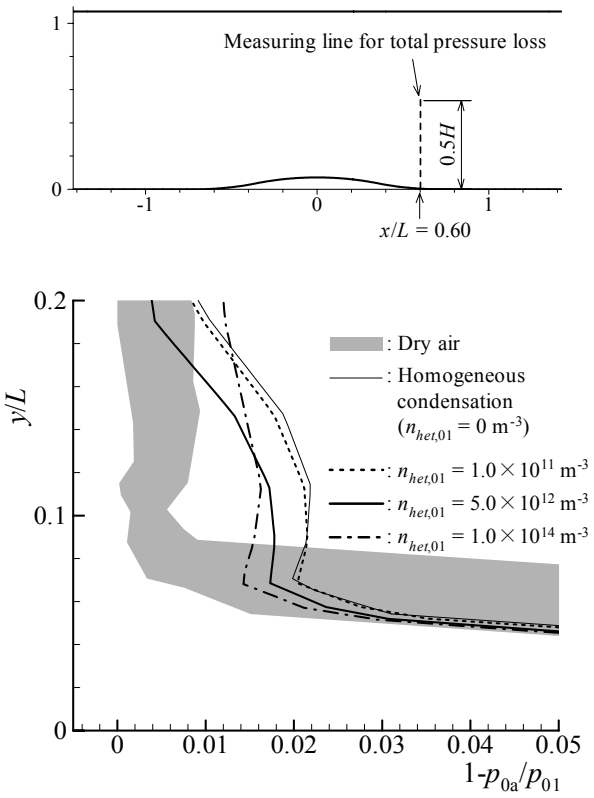

Fig 6. Distributions of total pressure loss (x/L = 0.60)

Figure 6 shows the distributions of total pressure loss ($1-p_{0a}/p_{01}$, p_{0a} : local total pressure, p_{01} : total pressure in the reservoir) on measuring line (x/L = 0.60) indicated in the upper part of this figure. The distribution for case with the periodic oscillation of the shock wave (dry air) is also shown in it, for reference. In cases of $n_{het,01}$ =0 m^{-3} (homogeneous condensation) and 1.0×10^{11} m^{-3}, there is not difference in the distributions of the total pressure loss. The total pressure loss in the region of y/L < 0.12 is the largest for case of $n_{het,01}$ =0 m^{-3} (homogeneous condensation) and 1.0×10^{11} m^{-3}. In this region, the condensate mass fraction increases in the order of $n_{het,01}$ = 1.0×10^{14} m^{-3}, 5.0×10^{12} m^{-3}, 1.0×10^{11} m^{-3} and 0 (homogeneous condensation). For y/L > 0.18, the total pressure loss for $n_{het,01}$ = 5.0×10^{12} m^{-3} , 1.0×10^{11} m^{-3} and 0 m^{-3} approaches to that for case of dry air. However, for $n_{het,01}$ = 1.0×10^{14} m^{-3}, it is the largest in this range. This is because the amount of the condensate mass fraction induced by the heterogeneous condensation is larger in comparison with the cases for $n_{het,01}$ = 1.0×10^{11} m^{-3} and 5.0×10^{12} m^{-3}.

Total pressure losses were integrated from the wall surface to the center (y/L = 0.536) of the main flow at the position (x/L = 0.60) as shown in Fig.6. Table 1 shows the ratio of integrated total pressure loss for each case to the average value of the integrated total pressure loss for the case of S_{01} = 0. As seen from this table, the variation of the integrated total pressure loss in case of S_{01} = 0 distributes in the large range. In the case of homogeneous condensation, it becomes small about 23.4 % in comparison with the average value for S_{01} = 0. In the

Table 1: Integrated total pressure loss ($x/L = 0.60$)

	Total pressure loss (%)		
$S_0 = 0$ (Dry air)	Minimum	Average	Maximum
	57.0	100	150
$n_{het,01} = 0$ m^{-3} (Homogeneous condensation)	76.6		
$n_{het,01} = 1.0 \times 10^{11}$ m^{-3}	80.3		
$n_{het,01} = 5.0 \times 10^{12}$ m^{-3}	67.1		
$n_{het,01} = 1.0 \times 10^{14}$ m^{-3}	88.0		

cases of heterogeneous condensation, the integrated total pressure losses in each case also become small in comparison with the average value for $S_{01} = 0$. Particularly, for the case of $n_{het,01} = 5.0 \times 10^{12}$ m^{-3}, it shows minimum value. However, in the cases of $n_{het,01} = 1.0 \times 10^{11}$ m^{-3} and 1.0×10^{14} m^{-3}, the integrated total pressure losses becomes large in comparison with the case of homogeneous condensation. This means that the suitable solid particle concentration exists for minimization of the total pressure loss.

5. CONCLUSIONS

The effect of the heterogeneous condensation on the characteristics of the unsteady adiabatic shock wave generated on the bump model in the transonic flow field was investigated numerically. The result obtained showed the oscillation of the shock wave was suppressed completely regardless of the condensation (nucleation) process. The shock strength was reduced with an increase of the solid particle concentration. Total pressure loss near the bump wall was strongly dependent on the concentration of the solid particles per unit volume, and there existed the suitable solid particle concentration for minimization of the total pressure loss.

6. REFERENCES

1. Matsuo, S., Setoguchi, T., Yamashita, H., Kaneko, K., Kim, H.D., and Matsuo, K., 2001, "Control of Shock Wave Using Nonequilibrium Condensation of Moist Air," *Proceedings of Experimental Heat Transfer, Fluid Mechanics, and Thermodynamics*, pp. 1841-1846.
2. Shimamoto, K., Matsuo, S., Setoguchi, T., Tanaka, M., and Kaneko, K., 2002, "Control of Shock Wave in Transonic Flow Field," *Proceedings of the Fifth JSME-KSME Fluids Engineering Conference*, on Disc[CD-ROM].
3. Wegener, P.P., and Mach, L.M., 1958, "Condensation in Supersonic Hypersonic Wind Tunnels," Advances in Applied Mechanics, Vol.5, Academic Press.
4. Kotake, S., and Glass, I.I., 1976, "Condensation of Water Vapour on Heterogeneous Nucleation in a Shock Tube," UTIAS Report, No. 207.
5. Sislian, J.P., 1975, "Condensation of Water Vapor with or without a Carrier Gas in a Shock Tube," UTIAS Report, No. 201.
6. Heiler, M., 1999, "Instationäre Phänomene in homogen/heterogen kondensierenden Düsen- und Turbinenströmungen," Dissertation, Fakultät für Maschinenbau, Universität Karlsruhe(TH), Germany.
7. Yee, H.C., 1989, "A Class of High-Resolution Explicit and Implicit Shock Capturing Mthods," NASA TM-89464.
8. Baldwin, B.S., and Lomax, H., 1978, "Thin Layer Approximation and Algebraic Model for Separated Turbulent Flows," AIAA paper, No. 78-257.

7. NOMENCLATURE

Symbol	Meaning	Unit
A_e	Surface area of solid particle on which the vapor can nucleate	(m^2)
$\boldsymbol{E}$, $\boldsymbol{F}$	Inviscid flux vectors	(-)
E_t	Total energy per unit volume	(J/m^3)
g	Condensate mass fraction	(-)
I	Nucleation rate per unit time and volume	(1/s·m^3)
$\tilde{I}$	Nucleation rate per unit time and area	(1/m^2)
k	Thermal conductivity	(W/m·K)
k_{het}	Number of embryos per unit volume	(m^{-3})
n_{het}	Number of embryos per unit mass	(kg^{-1})
n_{hom}	Number of nuclei per unit volume	(m^{-3})
p	Pressure	(Pa)
$\boldsymbol{Q}$	Source term of condensation	(-)
r	Radius	(m)
r^*	Critical radius	(m)
$\boldsymbol{R}$, $\boldsymbol{S}$	Viscous flux vectors	(-)
Re	Reynolds number	(-)
R_p	Radius of a solid particle	(m)
t	Time	(s)
T	Temperature	(K)
u, v	Velocity components	(m/s)
$\boldsymbol{U}$	Conservative vector	(-)
x, y	Cartesian coordinates	(m)
Symbols		
ρ	Density	(kg/m^3)
τ	Shear stress	(Pa)
τ_t	Time	(s)
Subscripts		
01	Reservoir	
0a	Local	
emb	Embryo	
hom	Homogeneous	
het	Heterogeneous	
l	Liquid	
m	Mixture	
nuc	Nucleus	
r	Droplet of radius *r*	
s	Saturation	
total	Total	